Amyloid Fibril Formation by a Synthetic Peptide from a Region of Human Acetylcholinesterase that Is Homologous to the Alzheimer's Amyloid-β Peptide[†]

Matthew G. Cottingham, Michael S. Hollinshead, and David J. T. Vaux*

Sir William Dunn School of Pathology, University of Oxford, Oxford OX1 3RE, U.K.

Received April 26, 2002; Revised Manuscript Received June 25, 2002

ABSTRACT: A region near the C-terminus of human acetylcholinesterase (AChE) is weakly homologous with the N-terminus of the Alzheimer's disease amyloid-β peptide. We report that a 14-amino acid synthetic polypeptide whose sequence corresponds to residues 586−599 of the human synaptic or T form of AChE assembles into amyloid fibrils under physiological conditions. The fibrils have all the classical characteristics of amyloid: they have a diameter of 6−7 nm and bind both Congo red and thioflavin-T. Furthermore, the kinetics of assembly indicate that fibril formation proceeds via a two-step nucleation-dependent polymerization pathway, and a transition in the peptide conformation from random coil to β-sheet is observed during fibril formation using far-UV circular dichroism spectroscopy. We also show that the peptide in aggregated fibrillar form has a toxic effect upon PC-12 cells in vitro. AChE normally resides mainly on cholinergic neuronal membranes, but is abnormally localized to senile plaques in Alzheimer's disease. Recently, an in vitro interaction between AChE and Aβ, the principal constituent of the amyloid fibrils in senile plaques, has been documented. The presence of a fibrillogenic region within AChE may be relevant to the interaction of AChE with amyloid fibrils formed by Aβ.

The formation of insoluble proteinaceous aggregates known as amyloid fibrils is characteristic of at least 20 slow-onset degenerative diseases (*1*). The deposits formed in these "amyloidoses" have common morphological and tinctorial properties: they are composed ultrastructurally of straight, unbranched fibrils with a diameter of 5−10 nm and bind the traditional histochemical stains for amyloid, the fluorescent benzothiazole thioflavin-T, and the diazobenzidine dye Congo red, which has a characteristic apple-green birefringence when imaged under cross-polarizers (*2*). Despite these similarities, the major polypeptide constituents of the fibrillar deposits associated with the various amyloid diseases have widely differing sequences, sizes, and native conformations. For example, the intact globular proteins transthyretin and lysozyme (*3*) are deposited as amyloid in familial amyloid polyneuropathy and hereditary systemic amyloid, whereas type II diabetes is associated with amyloids composed of a short peptide known as islet amyloid polypeptide (*4*).

The structure and assembly of amyloid fibrils formed by a number of polypeptides have been extensively studied in the laboratory (*5*, *6*). The kinetics of aggregation are typical of nucleation-dependent polymerization, with a critical concentration above which the unassembled polypeptide exists in a metastable state, requiring an unfavorable nucleation event for initiating rapid polymerization (*6*). In the case of folded proteins, as opposed to natively unfolded peptides, partial denaturation by chemical destabilization of the native fold may be required before the protein can self-assemble (*7*). Synthetic amyloid fibrils formed in vitro have the same ultrastructural and tinctorial properties as those found in a pathological setting, and have furthermore been shown to be toxic to tissue culture cells, indicating that fibril formation and amyloid deposition may have aetiological significance (*8*). X-ray diffraction analysis, circular dichroism spectroscopy and Fourier transform infrared spectroscopy have revealed that amyloid has a generic "cross-β" conformation, composed of multiple copies of the constituent polypeptide arranged into stacked β-sheets running perpendicular to the fibril axis (*9*−*11*). These observations suggest an explanation for the ability of different proteins with unique native conformations to adopt an essentially identical structure: the formation of amyloid may not be a peculiarity of the proteins that form fibrils in vivo, but rather a generic property of all polypeptide chains, albeit one which evolution has presumably not favored (*12*, *13*). Indeed, Dobson and co-workers have recently described several proteins that are not known to be associated with any pathological process, but which can be induced to form amyloid fibrils under laboratory conditions (*14*−*17*). However, since not all proteins are associated with amyloidosis, there is some selectivity with respect to which polypeptides are capable of forming amyloid in vivo rather than under the overtly nonphysiological laboratory conditions sometimes required to generate amyloid fibrils.

Intra- and extracellular amyloid deposits called neurofibrillary tangles and senile plaques, respectively, are associated with the most prevalent form of senile dementia, Alzheimer's disease. Together with extensive neuronal loss, they are the hallmark neuropathological features of the disease and are still the only means of confirming diagnosis post-mortem. Neurofibrillary tangles consist primarily of hyperphosphorylated tau, while the major fibrillar component of senile

[†] This work was supported by a research grant from Synaptica Ltd., a spin-out company from the University of Oxford.

* To whom correspondence should be addressed. Telephone: +44-(1865)275544. Fax: +44(1865)275501. E-mail: vaux@molbiol.ox.ac.uk.

10.1021/bi0260334 CCC: $22.00
Published on Web 10/26/2002

plaques is the amyloid-β peptide (Aβ), a 40−42-amino acid fragment of the Alzheimer precursor protein (APP). Analysis of genetic mutations that are responsible for very rare familial forms of the disease has led to the development of the amyloid cascade hypothesis, currently the most widely accepted model of the aetiology of Alzheimer's disease (*18*). It proposes that the key toxic insult is the formation and deposition of amyloid fibrils by the normally soluble Aβ peptide, as a result of its overproduction by aberrant proteolytic events and its interactions with so-called pathological chaperones. Apolipoprotein E and antichymotrypsin are two such proteins: they are minor constituents of senile plaques and have allelic variants that are capable of increasing the proclivity of Aβ to assemble into amyloid fibrils. Other proteins that are found to be abnormally associated with senile plaques in Alzheimer's disease (*19*−*21*) are acetylcholinesterase (AChE, EC 3.1.1.8) and the evolutionarily related enzyme butyrylcholinesterase (BuChE, EC 3.1.1.7). AChE is well-known as the enzyme responsible for the hydrolysis of the neurotransmitter acetylcholine at cholinergic synapses and neuromuscular junctions in the mammalian nervous system (*22*). The function of BuChE remains unclear, and it is normally expressed only at very low levels in the brain (*23*). There are other links between AChE and Alzheimer's disease, apart from its presence in senile plaques (*24*−*26*). There is a huge loss of AChE and choline acetyltransferase activity (*27*, *28*) which correlates with the severity of Alzheimer-type neuropathology in the affected areas (*29*). Furthermore, the degeneration of the cholinergic system is more pronounced and occurs earlier than that of other neurotransmitter systems, and there is a very high, though not perfect, correlation between areas that have high levels of AChE and areas which degenerate in Alzheimer's disease (*30*, *31*).

Several recent publications by Inestrosa and co-workers (*32*, *33*) have demonstrated an interaction in the laboratory between AChE and fibrillar Aβ, in addition to showing evidence that AChE behaves in vitro rather like a pathological chaperone, in that it is capable of increasing the rate of fibril formation by Aβ (*34*, *35*) and the neurotoxicity of the fibrils (*36*). However, BuChE did not exhibit any interaction with Aβ (*33*), even though BuChE is also reported to be associated with amyloid plaques (*21*). The observation, based on the use of butyrylthiocholine, a substrate which cannot be hydrolyzed by AChE, appears to be robust: even though the AChE associated both with synthetic (*34*) and Alzheimer's disease amyloid is known to have altered characteristics [including kinetic parameters (*37*), optimum pH (*38*), and inhibitor sensitivity (*39*)], its substrate specificity, a property enshrined in the structure of the catalytic gorge (*40*), has not been reported to be altered.

The central theme of the current investigation concerns the means by which AChE might interact with Aβ. One possibility is a heterotypic interaction between Aβ and some site on the well-known native globular structure of AChE: a region known as the peripheral anionic site has recently been proposed to be the area responsible for interactions with Aβ (*41*). But since amyloid fibrils have a generic structure, which can be adopted by multiple proteins in vivo, and possibly by any protein under the right nonphysiological conditions in vitro, and which is based on homotypic interactions between multiple copies of an identical polypeptide, it is conceivable that interactions of other proteins with an amyloid deposit consisting principally of Aβ may occur by an "allotypic" interaction, in which both proteins adopt the generic cross-β structure to form part of an amyloid fibril with a mixed composition. Clearly, while any protein may be able to be induced to form fibrils in vitro, not all proteins associate with Aβ, so if the basis of an interaction is indeed the adoption of the same nonunique three-dimensional structure by the two polypeptides, there should be some underlying explanation for the specificity of the interaction at the level of primary structure. In this paper, this possibility is investigated by comparison of the amino acid sequences of AChE and APP, and a short homologous region is identified, lying near the N-terminus of Aβ. Subsequent biophysical studies of a synthetic peptide designed around the homologous region of AChE reveal that it is a novel fibrillogenic peptide capable itself of forming, under physiological conditions, aggregates with all the typical ultrastructural, morphological, tinctorial, and toxicological characteristics of amyloid.

EXPERIMENTAL PROCEDURES

Sequence Analysis. The sequence alignment software dotter (*42*) was used to analyze the protein sequences of human APP and human synaptic or T form (containing exon 6) AChE (*23*). The program compares the sequences in all possible registers and outputs a dot matrix showing homologous regions as diagonal rows of high scores. The score is calculated by averaging the pairwise matches over a 25-amino acid sliding window, and is represented by the grayscale intensity in the dot matrix output.

Synthetic Peptides. The peptide AEFHRWSSYMVHWK ($AChE_{586-599}$), prepared as a trifluoroacetate salt, was synthesized and purified via HPLC to >95% by M. Pitkeathley at the Oxford Centre for Molecular Sciences (OCMS, Central Chemistry Laboratory, Oxford University) using standard fmoc methodology. The >95% pure N-terminally biotin-6-amidocaproylated, C-terminally amidated $AChE_{586-599}$ (Bi-$AChE_{586-599}$-Am) was purchased from Ansynth B.V. (Roosendaal, The Netherlands). The peptides were dissolved in ultrapure water, divided into small aliquots, and relyophilized. An aliquot was freshly redissolved in water for each series of experiments. $A\beta_{25-35}$ was prepared at OCMS and treated in the same way.

Turbidimetry. A fresh 1 mM solution of the peptide was diluted to 400 μM in polystyrene semi-micro cuvettes, and 20 mM sodium phosphate (pH 7.0) was added to further dilute the peptide to 200 μM. The absorbance at 450 nm of two samples was immediately read at 25 °C in a Jenway 6100 spectrophotometer, and readings were taken every 10 min after briefly mixing the samples by inversion for $AChE_{586-599}$, or every 30 s without mixing for Bi-$AChE_{586-599}$-Am. For the pH range, the peptides were prepared in duplicate at pH 6.0, 7.0, and 8.0 in 10 mM sodium phosphate, at pH 9.0 and 10.0 in 10 mM sodium glycinate, and at pH 12.0 by titration with NaOH. The solutions were incubated in a sealed 96-well plate for 18 h at 25 °C, and the absorbances at 450 nm were read in a BMG Polarstar plate reader.

Electron Microscopy. A 200 μM solution of the peptide was prepared in 10 mM sodium phosphate (pH 7.0) and

incubated overnight at 25 °C. The fibrils were adsorbed onto freshly glow discharged Formvar-coated grids and negatively stained with 1% phosphotungstic acid (pH 7.0). Electron micrographs were acquired using a Zeiss 912 Omega transmission electron microscope equipped with a 2K × 2K digital camera.

Circular Dichroism. Far-UV CD spectra were obtained using a Jasco J-720 specropolarimeter and cuvettes with a path length of 1 mm at 25 °C. Peptide solutions (200 μM) in 10 mM sodium phosphate (pH 7.0) or in water were prepared as described above, and spectra were recorded immediately, 90 min, 3 h, 18 h, and 5 days after neutralization. Background spectra recorded in the absence of peptide were subtracted from the sample spectra.

Thioflavin-T Fluorescence. Fluorescence spectra of thioflavin-T were acquired at 25 °C with a Perkin-Elmer LS50B fluorescence spectrometer. A 200 μM solution of peptide in 10 mM sodium phosphate (pH 7.0) was incubated overnight, and 6.25 μL of 2.5 mM thioflavin-T (Sigma) in phosphate-buffered saline was added to 250 μL of the peptide solution. Control spectra of thioflavin alone and peptide alone were recorded. Excitation at 440 nm (slit, 5 nm) was used during collection of the emission spectrum, while the emission was monitored at 482 nm (slit, 10 nm) for the excitation spectrum. Kinetic thioflavin-T assays were performed at 25 °C in a BMG Polarstar 96-well plate reader. Thioflavin (2.5 μL) was pipetted into the wells of a black-walled 96-well plate, and 100 μL of a solution of the peptide at a final concentration of 200 μM was added to the wells within a few seconds of neutralization with an equal volume of 20 mM sodium phosphate (pH 7.0). Control wells contained thioflavin only or peptide only. The fluorescence intensity was measured immediately and every 15 min for 18 h ($AChE_{586-599}$) or every 30 s for 1 h (Bi-$AChE_{586-599}$-Am) using a 450 nm excitation filter (bandwidth, 10 nm) and a 485 nm emission filter (bandwidth, 15 nm). Each data point is the average of the fluorescence intensity over ten 50 Hz xenon bulb flashes.

Congo Red Binding. A 200 μM solution of the peptide in 10 mM phosphate (pH 7.0) was incubated overnight at 25 °C. The solution was mixed to resuspend the precipitated peptide, and an absorbance spectrum from 400 to 700 nm was collected with a Beckmann DU600 spectrophotometer using polystyrene semi-micro cuvettes. Congo red was added to a final concentration of 5 μM, and the spectrum was recorded after incubation for 10 min. A third spectrum of the unbound dye was also collected. The spectrum of peptide alone was subtracted from the spectrum of Congo red with peptide to correct for the turbidity of the sample due to the precipitated peptide. A similar pair of cuvettes containing 10 μM Congo red were photographed. It was determined that >95% of the 10 μM Congo red was bound to the 200 μM peptide by pelleting the aggregates in a microcentrifuge for 5 min at 15 000 rpm and measuring spectrophotometrically the concentration of Congo red in the supernatant.

MTT Cytotoxicity Assay. Rat pheochromocytoma PC-12 cells were cultured in DMEM with 10% fetal calf serum (FCS), 5% horse serum, and 2 μM glutamine and were seeded into collagen-coated 96-well plates in 100 μL of medium per well. The following day the cells were washed once with DMEM before addition of peptide solutions prepared in water and mixed with an equal volume of 2× DMEM containing 2% glutamine and 4 μM insulin. All experiments were performed in triplicate. After 48 h, 10 μL of a 5 mg/mL solution of 3-(4,5-dimethylthiazol-2-yl)-2,5-diphenyltetrazolium bromide (MTT) was added, and the cells were incubated for a further 4 h. The reduced dye was dissolved by adding 100 μL of 10% SDS in 0.01 M HCl and incubating the plates overnight at 37 °C, before the absorbances were read at 550 nm. The data are expressed as the percentage MTT reduction observed compared to control after subtraction of a zero value obtained in the presence of 0.1% Triton X-100.

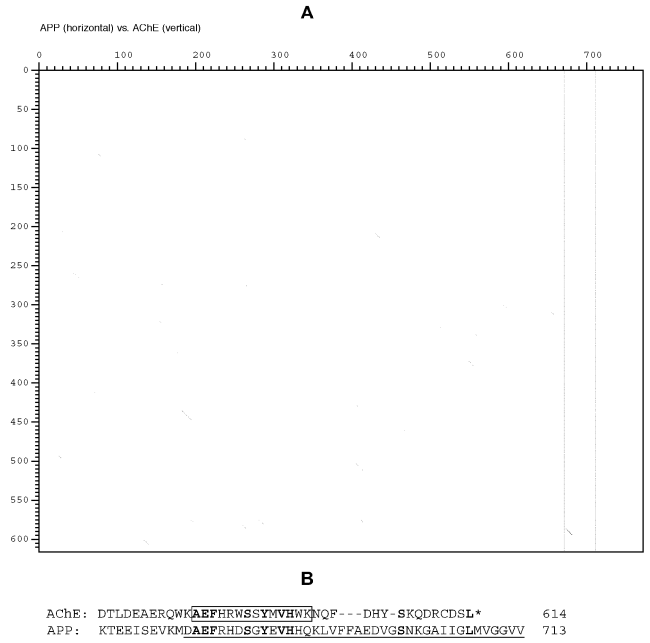

FIGURE 1: Sequence alignment of APP and AChE. (A) Output of dotter software using APP as the horizontal sequence and AChE as the vertical sequence. The vertical lines indicate the positions of the cleavage sites which give rise to Aβ. The most intense and the longest diagonal row of high scores lies near the N-terminus of Aβ. (B) Sequence alignment at the region of interest. Identical residues are in bold type; Aβ is underlined, and the 14-amino acid synthetic peptide ($AChE_{586-599}$) designed to encompass the region of similarity and used in this study is shown boxed.

RESULTS

Sequence Comparison of AChE and APP. The sequence analysis software dotter (*42*) was used to search for regions of sequence similarity between human AChE and human APP. The dot matrix output, shown in Figure 1A, identifies the longest and highest-scoring region of similarity lying near the N-terminus of Aβ, the 40−42-amino acid fragment of APP, and within the 40-amino acid C-terminal oligomerization domain, encoded by exon 6 (*23*), of the synaptic or T form of AChE. Other matches, lying outside the Aβ fragment, either have lower scores, indicated by the lower intensity, or are discontiguous. On the basis of this result, a 14-amino acid synthetic peptide was designed to include the region of interest within a hypothetical tryptic fragment; this peptide ($AChE_{586-599}$), corresponding to residues 586−599 of human T form AChE, is indicated by a box in the sequence alignment in Figure 1B.

It soon became clear that the similarity between AChE and APP in this region goes beyond sequence homology:

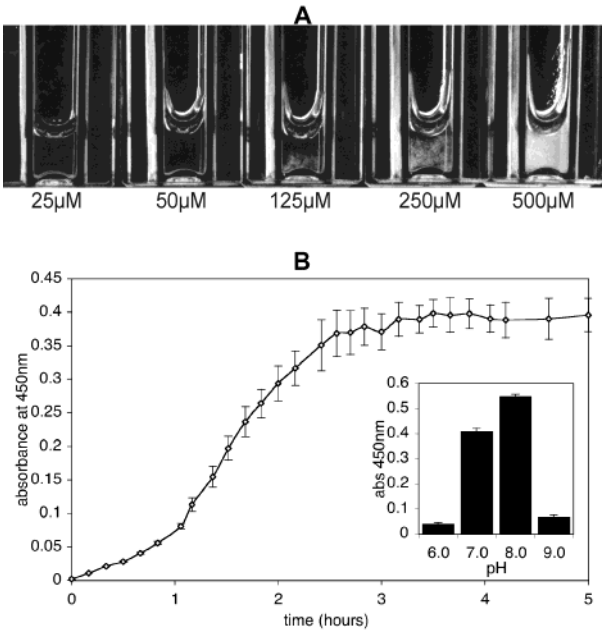

FIGURE 2: Precipitation of $ACHE_{586-599}$. (A) Peptide at a range of concentrations after overnight incubation in PBS. The critical concentration for precipitation is 50 μM. (B) Increase in turbidity measured by light scattering at 450 nm of 200 μM peptide after neutralization to pH 7.0. In the inset of panel B is shown the turbidity at 450 nm of 200 μM solutions of peptide B after overnight incubation over a pH range. The peptide only aggregates above pH 6 and below pH 9. Error bars are the standard error of the mean value of two samples; data that are shown are one representative experiment from multiple repetitions.

the $ACHE_{586-599}$ peptide is capable, like Aβ, of forming amyloid fibrils in vitro. There is no single method that is able to uniquely identify amyloid: instead, an operational definition has evolved, based on multiple common properties of amyloid fibrils (*6*, *17*). We have therefore used a range of techniques to demonstrate that $ACHE_{586-599}$ forms, at neutral pH in aqueous solution, precipitates consisting of classical amyloid fibrils. The peptide aggregates in phosphate-buffered saline (PBS), as shown in Figure 2A, but the other data that are shown were gathered in the absence of physiological salt, because it was found to increase noise in the far UV in CD spectra. So that the results are comparable, salt was also omitted from buffers used in the other kinetic experiments shown here, since the only observed effect of physiological concentrations of salt in all the systems that were studied was to slightly increase the rate of fibril formation.

Turbidimetry and Precipitation. The tendency of $ACHE_{586-599}$ to aggregate is highly dependent upon pH. The peptide appears to be entirely soluble in water at concentrations up to $\geq$10 mM; however, because the peptide is synthesized as a trifluoroacetic acid salt, the pH of an aqueous solution is low ($<$6 at micromolar concentrations and $<$4 at 10 mM). Only when the solution is neutralized does the peptide rapidly aggregate and form a precipitate. Under physiological conditions, in PBS, there is a critical concentration for aggregation of $\sim$50 μM, below which precipitation does not occur (Figure 2A). Precipitation occurs over a time period of several hours: Figure 2B shows the time course of the increase in turbidity, monitored by optical density at 450 nm, of a 200 μM solution of peptide immediately after neutralization to pH 7.0. A lag phase before the onset of assembly and precipitation is not apparent. There is a narrow pH window in which peptide aggregation is favored: it does not assemble into fibrils at or below pH 6 or at or above pH 9 (as shown in the inset of Figure 2B). Aβ has a critical aggregation concentration of 10$-$40 μM (*6*), and an insolubility window between pH 3.5 and 7.5 with a maximum at pH 5$-$6 (*43*). $ACHE_{586-599}$ therefore has a slightly higher critical concentration than Aβ and aggregates at neutral pH, rather than under mildly acidic conditions.

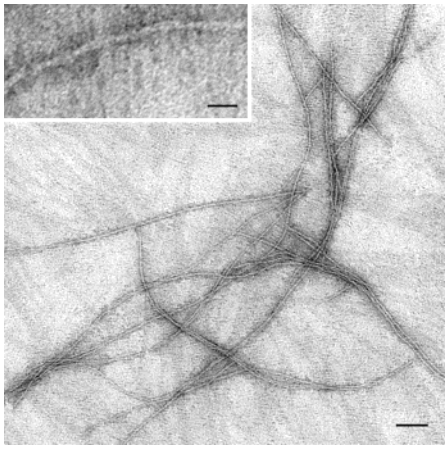

FIGURE 3: Transmission electron micrograph of $ACHE_{586-599}$ aggregates. Main image scale bar of 100 nm; inset scale bar of 20 nm. The fibrils measure 6$-$7 nm in diameter. The peptide was incubated overnight at 200 μM in 10 mM phosphate (pH 7.0) before being absorbed to EM grids and negatively stained.

Precipitated $ACHE_{586-599}$ can be readily redissolved by addition of acid or base to bring the pH away from neutral (data not shown), indicating that the assembly of the peptide into fibrils is reversible. In the case of Aβ, high (*44*, *45*) and low pH (*46*, *47*) can be employed to dissolve pre-existing fibrillar aggregates present in stocks of the synthetic peptide, and acidic denaturing conditions are employed in the extraction and purification of fibrillar Aβ from biological samples (*48*).

Electron Microscopy. When the $ACHE_{586-599}$ aggregates are examined by negative staining followed by electron microscopy, they are seen to consist of amyloid-type fibrils measuring anything up to several micrometers in length with a diameter of 5$-$7 nm (Figure 3). The fibrils may be single fibers, a pair twisted into a helix, or a complex interlocking mat. No such fibrils are seen on EM grids prepared from nonturbid solutions of unprecipitated peptide.

Circular Dichroism. Figure 4 shows the kinetic CD analysis of 200 μM $ACHE_{586-599}$ buffered at pH 7.0 and without buffering, where the pH is 5$-$6, because of the presence of residual trifluoroacetic acid. After neutralization, there is a clear and gradual transition over an 18 h period from a spectrum whose maximum at $\sim$225 nm and minimum at $\sim$200 nm are indicative of a high degree of random coil conformation to a spectrum with a minimum at $\sim$215 nm and a maximum at $\sim$195 nm, which is diagnostic of β-sheet secondary structure (Figure 4A). Amyloid is highly β-sheet rich, and has a generic cross-β structure (*5*). In the unbuffered lower-pH state, the spectrum does not change with time, and the peptide remains unstructured and nonfibrillar (Figure 4B). The experiment was continued out to 5 days, but no further changes in the CD spectra were observed after 18 h (data not shown). The presence of a single isodichroic point at

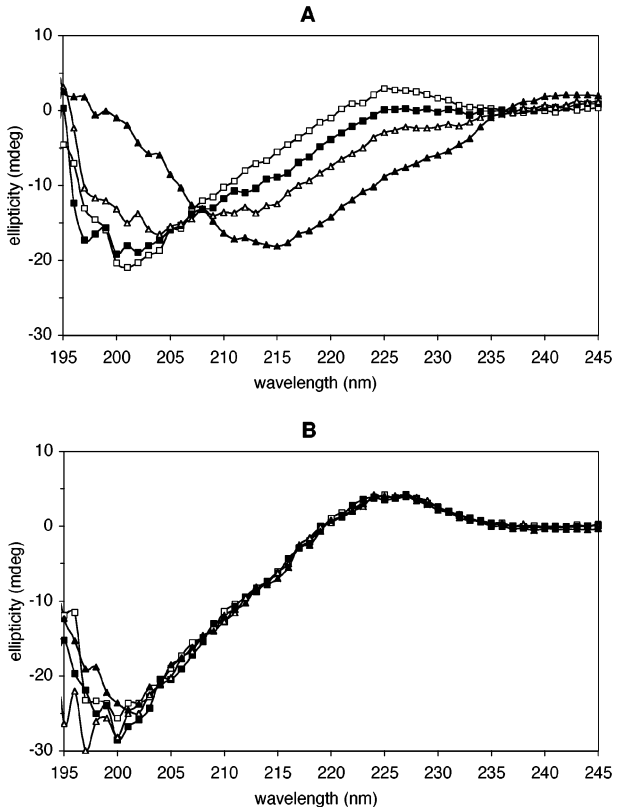

FIGURE 4: Circular dichroism spectra of $AChE_{586-599}$. Spectra were recorded at 1 min (□) 90 min (■), 3 h (△), and 18 h (▲) after dilution of the peptide into 10 mM phosphate (pH 7.0) (A) or into water (B), where the pH after peptide addition was 5−6 due to residual trifluoroacetic acid in the preparation. At neutral pH, the peptide forms amyloid fibrils and shows a transition from random coil to β-sheet secondary structure, whereas at lower pH, the peptide has a stable random coil conformation and does not form fibrils. The data that are shown are one representative experiment from multiple repetitions.

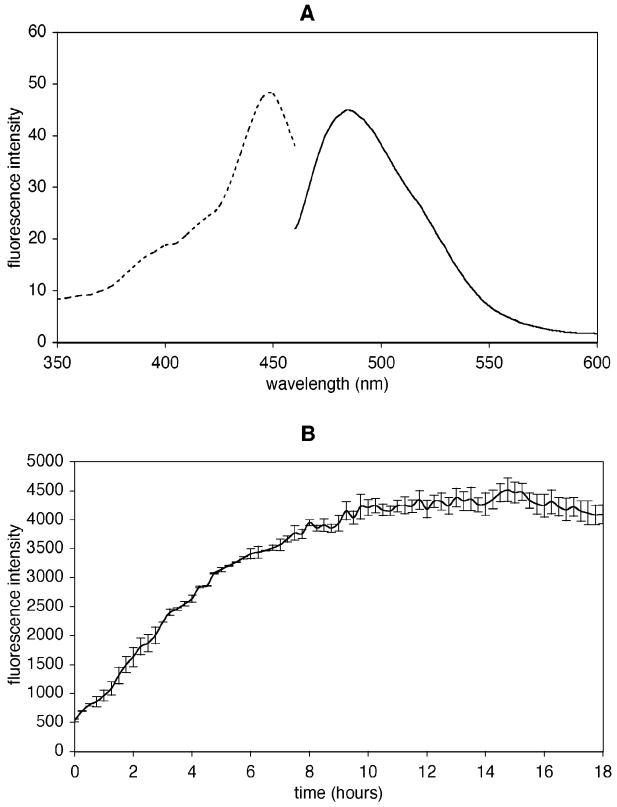

FIGURE 5: Binding of thioflavin-T to $AChE_{586-599}$ fibrils. (A) Fluorescence spectrum of thioflavin-T in the presence of 200 μM peptide aged for 24 h in 10 mM phosphate (pH 7.0). Excitation spectrum (- - -) with emission monitored at 482 nm and emission spectrum (—) with excitation at 442 nm. The excitation and emission peaks show the classic red shift (*49*) compared to the free dye (data not shown) which has excitation and emission peaks at 340 and 430 nm, respectively. (B) Increase in ThT fluorescence during fibril formation after dilution of peptide B at 200 μM into 10 mM phosphate (pH 7.0). Excitation at 450 nm and emission at 485 nm. Values are the means of two samples, and error bars are the standard error of the mean; the data that are shown are from one representative experiment from multiple repetitions.

207−208 nm in the neutral-pH CD spectra indicates that the kinetics at least approximate those of a first-order process.

Thioflavin-T Fluorescence. The fluorescent benzothiazole dye thioflavin-T (ThT) has long been used to study amyloid deposition in a pathological context. When the dye binds to amyloid fibrils, there is a characteristic shift in the fluorescence excitation and an increase in emission intensity (*49*). Fibrillar $AChE_{586-599}$ causes exactly such changes in the spectral properties of the dye (Figure 5A): the excitation and emission maxima are red shifted from 340 and 430 nm to 450 and 490 nm, respectively, together with an increase in the fluorescence intensity. The time course of assembly can be monitored by selective excitation of the bound dye. After neutralization of 200 μM peptide, the fluorescence of the bound dye immediately begins to increase as fibrils are formed, and reaches a plateau after ~12 h (Figure 5B).

There is a disparity between the rate of precipitation monitored spectrophotometrically and the rate of acquisition of thioflavin-T binding capability or β-sheet secondary structure (compare Figures 2B and 5B). Turbidimetry detects particles with a hydrodynamic radius greater than the wavelength of incident light (in this case 450 nm), but since fibrils have a complex, nonhomogeneous structure, it is hard to evaluate the significance of the turbidity measurements. Thioflavin-T fluorescence and conformational changes are therefore more faithful measures of the rate of fibril extension.

Congo Red Binding. Congo red, like thioflavin, is widely used as a histological indicator of amyloid deposition. The binding interaction is characterized by apple-green birefringence and a metachromatic shift in the absorbance spectrum (*50*). Once again, fibrillar $AChE_{586-599}$ is seen to behave just like classical amyloid in that it too binds Congo red (Figure 6). The fibrils bind the dye and retain it as they precipitate out of solution; additionally, there is a marked red shift in the absorbance that can be seen with the eye as a change from an orange-red to a pink color, as well by examination of the absorbance spectrum. The spectrum shown has been corrected for turbidity caused by the precipitated fibrillar peptide.

MTT Cell Proliferation Assay. The reduction of the tetrazolium MTT by mitochondrial dehydrogenase activity is a widely used means of ascertaining cellular viability in vitro (*51*) and in PC-12 cells is an early indicator of β-amyloid-mediated cell death (*52*). The effect of $AChE_{586-599}$ and $A\beta_{25-35}$ on MTT reduction by PC-12 cells was compared (Figure 7). At 500 μM, the AChE peptide, like $A\beta_{25-35}$ at the same concentration, inhibits MTT reduction to ~40% of control values; however, at 5 μM, the effect of $AChE_{586-599}$

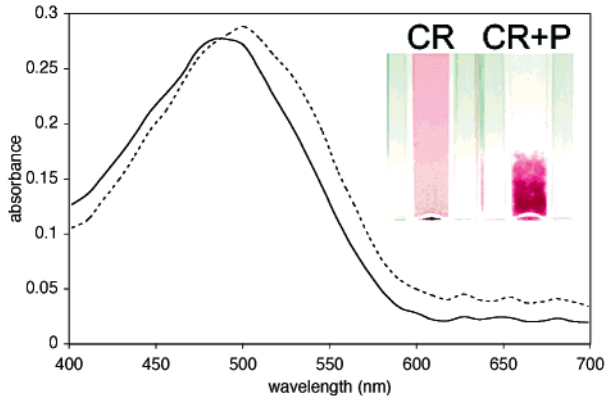

FIGURE 6: Binding of Congo red to $AChE_{586-599}$ fibrils. The graph shows the absorbance spectra of a 5 μM solution of Congo red (—) and 5 μM Congo red with 200 μM peptide [in 10 mM phosphate (pH 7.0), aged overnight and mixed], corrected for turbidity (- - -). The image shows 10 μM solutions of Congo red without and with 200 μM peptide, which has precipitated, bringing the dye with it. The absorbance spectrum of the Congo red bound to the peptide is red shifted, as is also apparent in the image, from an orange red to a rosy pink. At these concentrations, >95% of the Congo red is bound to the peptide.

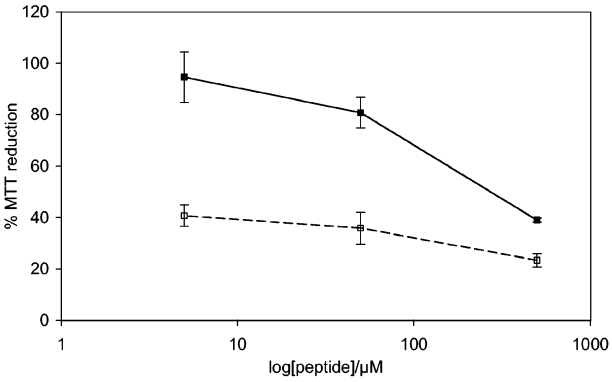

FIGURE 7: Cytotoxicity of $AChE_{586-599}$. Inhibition of MTT reduction by PC-12 cells upon application of $AChE_{586-599}$ (■) and $A\beta_{25-35}$ (□). The experiment was performed in triplicate, and the error bars represent the standard error of the mean. The data are scaled with respect to positive and negative controls at 0 and 100%, and are from one representative experiment of a set of three.

is negligible, but the value for $A\beta_{25-35}$ is still less than 40%. In a system where $A\beta_{25-35}$ has cytotoxic effects in concurrence with published observations (*52*), $AChE_{586-599}$ clearly exhibits similar toxicity, albeit at higher concentrations.

Modification of N- and C-Termini of $AChE_{586-599}$. The dependence of the aggregation of $AChE_{586-599}$ upon pH (Figure 1) indicates that charge plays a critical role in the process. The p*K* of histidine, of which there are two in $AChE_{586-599}$, is 6, so the deprotonation of their NH groups as the pH is increased toward neutral may be a crucial permissive step in the acquisition of fibrillogenic capability; second, the loss of positive charge at the amino terminus of $AChE_{586-599}$ might be expected to be involved in the preclusion of $AChE_{586-599}$ fibrillogenesis at pH ≥9, since the p*K* of the α-amino group is near 9. To investigate whether a free, charged amino terminus is required for assembly, and hence whether fibril formation by longer fragments of AChE or by the intact protein might be precluded, the fibrillogenic properties of a synthetic peptide having the same sequence, but an amidated C-terminus and a biotinylated N-terminus (Bi-$AChE_{586-599}$-Am), were also investigated. The p*K* of both biotin NH groups is >17 (*53*), so within the pH range of interest, there are no charges associated with the amino terminus. As shown in Figure 8, Bi-$AChE_{586-599}$-Am, when neutralized, forms Congophilic, thioflavin-T-binding, 7 nm amyloid fibrils even more rapidly than the unmodified peptide. It precipitates within seconds, as opposed to hours (compare Figures 2B and 8A), and thioflavin fluorescence reaches a plateau after ∼15 min, instead of ∼12 h (Figures 5 and 8C). Furthermore, the time courses of acquisition of thioflavin-T fluorescence and of turbidity match almost exactly in the case of Bi-$AChE_{586-599}$-Am, but do not in the case of the unmodified peptide, which is consistent with the formation of a larger number of shorter fibrils (with altered light scattering properties) as a result of an increased number of nucleation sites. The biotinylated peptide's extra hydrophobicity presumably accounts for these differences. The pH dependence of $AChE_{586-599}$ fibrillization is also altered by the modifications. While both peptides are soluble under mildly acidic conditions (≤pH 6), consistent with the idea that side chain charges on the histidine residues are involved, the biotinylated amidated peptide, unlike the unmodified peptide, is capable of self-assembly and precipitation at pH 9 and 10. Only when the pH is taken to 12 does Bi-$AChE_{586-599}$-Am remain soluble and nonfibrillogenic, suggesting that charges on the lysine and arginine (pK = 10.5 and 12.5) of $AChE_{586-599}$ may be involved in fibril formation. Free N- and C-termini are therefore not required for the fibrillogenic properties of $AChE_{586-599}$, though the deprotonization of the N-terminus is involved in the inhibitory effect of alkaline pH upon fibril formation by the unmodified peptide.

DISCUSSION

Identification of a Toxic Fibrillogenic Peptide Derived from AChE. AChE is heavily implicated in Alzheimer's disease (*25*), not least because it is abnormally localized in the amyloid fibril rich senile plaques characteristic of the disease (*19*, *20*). It has also been shown to interact in vitro with Aβ, the principal constituent of the plaques, and to increase its rate of assembly and its neurotoxicity (*32*−*36*). We analyzed the amino acid sequences of the splice variant of AChE found in the brain (*23*) and APP with the intention of searching for regions of sequence similarity that may be important for this interaction. A short homologous region was identified, lying near the N-terminus of Aβ (Figure 1), and a synthetic peptide, $AChE_{586-599}$, corresponding to the cognate region of AChE, was found to be capable of forming, under physiological buffering conditions, classical amyloid fibrils almost identical to those formed by Aβ. The fibrous precipitates formed by $AChE_{586-599}$ have all the characteristics of amyloid fibrils: they bind both Congo red (Figure 6) and thioflavin-T (Figure 5), have β-sheet secondary structure (Figure 4), are 5−7 nm in diameter (Figure 3), and exhibit typical kinetics of assembly (Figure 2). Furthermore, the fibrils have in vitro cytotoxic properties similar to those of $A\beta_{25-35}$ (Figure 7). It is, therefore, reasonable to consider that $AChE_{586-599}$ should be added to the growing list of amyloidogenic polypeptides.

Kinetics and pH Dependence of $AChE_{586-599}$ Aggregation. Self-assembly of amyloid in vitro proceeds via a nucleation-dependent polymerization process, with the following characteristics: (i) a critical concentration below which no

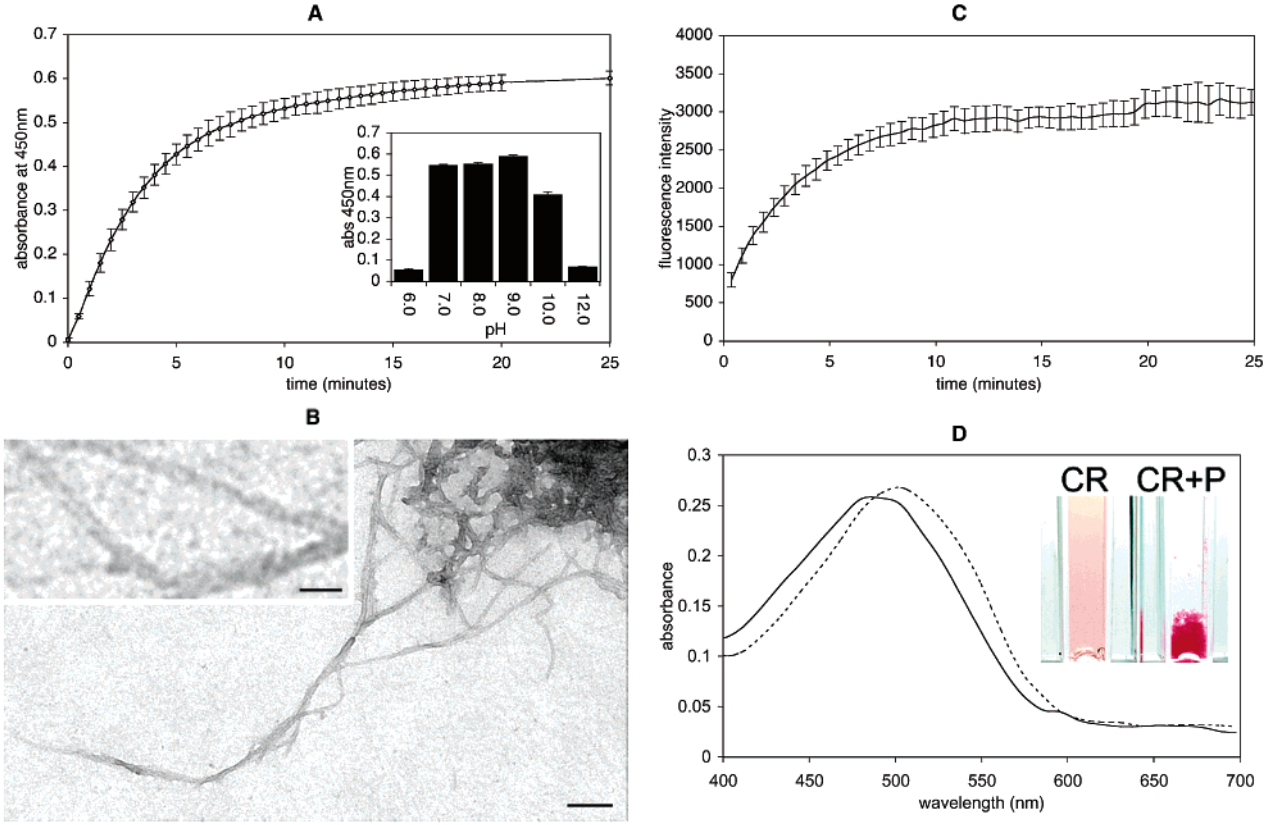

FIGURE 8: Fibrillogenic properties of biotinylated amidated $AChE_{586-599}$. (A) Time course of aggregation of Bi-$AChE_{586-599}$-Am after neutralization to pH 7.0 monitored by light scattering at 450 nm. The inset graph shows the final turbidity after overnight incubation across a pH range. (B) Transmission electron micrograph of negatively stained fibrillar aggregates of Bi-$AChE_{586-599}$-Am formed overnight at pH 7.0. The main image scale bar is 100 nm; the inset image scale bar is 20 nm. (C) Bi-$AChE_{586-599}$-Am fibril formation after neutralization to pH 7.0 monitored by thioflavin-T fluorescence (excitation at 450 nm and emission at 485 nm). (D) Absorbance spectra of 5 μM Congo red (—) and Congo red with aged fibrillar Bi-$AChE_{586-599}$-Am (- - -) corrected for turbidity. The inset image shows the Congo red associated with the precipitated fibrillar material and its change in color from orange-red to pink, which is also reflected in the absorbance spectra. The data shown in panels A and C are from one representative experiment of a series of three; the points are the means of two values, and the error bars represent the standard error of the mean. The concentration of Bi-$AChE_{586-599}$-Am was in all cases 200 μM.

aggregation occurs, (ii) a lag time before polymerization above the critical concentration, and (iii) a reduction in the lag time caused by addition of prepolymerized seeds (*6*).

$AChE_{586-599}$ has a critical concentration for aggregation of ~50 μM at pH 7, below which no fibrillar material is evident. This compares well with the published critical concentration of Aβ, which is 10−40 μM (*6*). Assembly is highly dependent upon pH as well as concentration: fibril formation is evident only within a narrow window above pH 6 and below pH 9 for the free peptide; modification of the N-terminus, as in Bi-$AChE_{586-599}$-Am, increases the upper limit of the window to pH 11. Because the peptide is synthesized as a salt of trifluoroacetic acid, the pH of unbuffered aqueous solutions of the peptide, which do not contain fibrillar material, always lies below pH 6. Aβ aggregation is favored under slightly more acidic conditions (between pH 3.5 and 7.5) compared to $AChE_{586-599}$, with a maximum near pH 5 (*43*, *44*).

There is no lag phase, at 200 μM, before the onset of fibril formation by $AChE_{586-599}$, when monitored by turbidity or thioflavin-T binding. The presence of a single isodichroic point in the CD spectra of $AChE_{586-599}$ also indicates that the conversion to β-sheet approximates a first-order process. It is possible that the formation of nuclei by $AChE_{586-599}$ is not particularly unfavorable under the given conditions, and occurs almost instantaneously. The length of the period of kinetic solubility can be extremely sensitive to concentration (*54*): Aβ does not have a lag phase at concentrations above 100 μM (*6*). An alternative possibility, which cannot be dismissed, is that oligomeric seeds are present in low-pH aqueous stock solutions, in which fibrils, nevertheless, do not form.

Relevance of the Sequence Similarity between $AChE_{586-599}$ and $A\beta_{1-16}$. The 16 amino-terminal residues of Aβ are not essential for the formation of fibrils by the peptide. The core fibrillogenic domain lies between residues 12 and 35: synthetic peptides corresponding to $A\beta_{25-35}$ are fibrillogenic (*55*), and deletions of N-terminal amino acids enhance the aggregation of Aβ peptides in vitro (*56*). $A\beta_{1-16}$ is nonfibrillogenic in our hands (data not shown) and in those of others (*35*). Nevertheless, there are some reports that the N-terminal region of Aβ is important in fibril formation: antibodies against EFRH (residues 2−5 of Aβ) can prevent self-aggregation of Aβ into amyloid (*57*), and structural changes in the region modulate Aβ fibrillogenesis (*58*, *59*). $A\beta_{1-16}$ is more charged and less hydrophobic than $AChE_{586-599}$: it has four additional charged residues (two aspartic acids, a glutamic acid, and a histidine) but two fewer tryptophans. It is possible that these differences account for the inability of $A\beta_{1-16}$ to form fibrils.

Interaction of AChE with Aβ. The 40-amino acid C-terminal tail, encoded by exon 6 of *ACHE* and running from position 575 to the end of the sequence of the synaptic (T) splice variant of AChE, is the domain responsible for oligomerization of the enzymatic subunits (*23*). The soluble enzyme may be G1 (monomeric), G2 (dimeric), and G4 (tetrameric), but G4 can additionally be anchored to the extracellular collagen subunit ColQ (*60*, *61*) or the membrane attachment subunit PRiMA (*62*). The conformation of the tail peptide is that of an amphipathic helix (*63*), with conserved aromatic residues on one face of the α-helix that are essential for the assembly of tetramers (*64*, *65*). The fibrillogenic region of residues 586−599 lies within this C-terminal oligomerization domain, but the $AChE_{586-599}$ peptide has, prior to fibrillogenesis, a random coil structure (Figure 4), rather than the native α-helical structure adopted by the same sequence in the parent protein. The native fold would probably require chemical disruption in the manner carried out for myoglobin and other proteins by Dobson et al. (*16*) before the whole protein or a conformationally stable fragment of the C-terminal tail would be expected to form amyloid fibrils in vitro. Nevertheless, the highly fibrillogenic properties of $AChE_{586-599}$ under physiological conditions suggest the intriguing possibility that the conversion of the α-helical tail of AChE to *β*-sheet by A*β*, acting at the region of residues 586−599, and the subsequent inclusion of the enzyme into a fibril of mixed proteinaceous origin, might account for the presence of the enzyme in senile plaques in Alzheimer's disease (*19*, *20*). The preservation, and indeed acceleration, of the fibrillogenic properties of the synthetic $AChE_{586-599}$ fragment in the N-terminally biotinylated and C-terminally amidated version of the peptide (Bi-$AChE_{586-599}$-Am) indicate that free N- and C-termini are not required for self-assembly into amyloid fibrils. This observation is compatible with the idea that the residues 586−599 of AChE, shown here to be highly fibrillogenic when present as a free fragment, may also be capable of adopting a non-native fibrillar structure when residing within the intact parent protein.

Several recent publications from the laboratory of Inestrosa (*41*) have focused on the interaction of AChE with A*β*, and home in on the peripheral anionic site, situated on the surface of the enzyme next to the entrance to the catalytic gorge (*66*), as the location of A*β* binding activity. This conclusion was based upon the ability of certain peripheral site ligands (*33*) and a monoclonal antibody against the peripheral site (*67*) to block the interaction of AChE with A*β*, as well as the absence of any interaction in vitro of A*β* with BuChE, which lacks the peripheral site (*33*). However, the peripheral and active site ligand BW284C51 did not block the interaction, the possibility of steric occlusion of another site by the antibody is not excluded, and BuChE is reported to be associated with A*β* in vivo (*21*). It is possible that $AChE_{586-599}$ may be an alternative or additional region responsible for the interaction of cholinesterases with senile plaques; this idea is currently under investigation. Two key predictions of this hypothesis would be (i) that a truncated form of AChE lacking the C-terminal oligomerization domain, and therefore the fibrillogenic region identified herein, would not be capable of interacting with A*β* and (ii) that the enzyme would be incapable of interacting with forms of A*β* lacking the homologous region present in residues 1−16.

G1 and G2 AChE Have an Exposed C-Terminal Tail. In Alzheimer's disease, there is a loss of membrane-bound G4 AChE associated with the degeneration of cholinergic axons, but there is also a smaller increase in the levels of the soluble G1 and G2 forms of the enzyme (*28*, *68*−*72*). Unlike the soluble G4 form, these forms are amphiphilic, as indicated by the difference in their sedimentation coefficients with and without the presence of detergents (*23*). The explanation for this observation is that the amphiphilic T-peptide oligomerization domains are hidden in the nonamphiphilic soluble tetrameric G4, but are exposed in the dimer and monomer, and are therefore able to interact with detergents (*60*, *61*). The above data suggest that the increase in Alzheimer's disease in the levels of the G1 and G2 forms results in an increased proportion of AChE that has an exposed C-terminal tail, and lead to the speculation that in Alzheimer's disease there may be an increased accessibility of the fibrillogenic region of AChE to heterologous interactions.

ACKNOWLEDGMENT

We thank the Oxford Centre for Molecular Sciences for access to CD spectroscopy and fluorimetry equipment and to custom peptide synthesis facilities.

REFERENCES

1. Kisilevsky, R., and Fraser, P. E. (1997) *Crit. Rev. Biochem. Mol. Biol. 32*, 361−404.
2. Kelly, J. W. (1997) *Structure 5*, 595−600.
3. Kelly, J. W. (1998) *Curr. Opin. Struct. Biol. 8*, 101−106.
4. Westermark, P., Wernstedt, C., Wilander, E., Hayden, D. W., O'Brien, T. D., and Johnson, K. H. (1987) *Proc. Natl. Acad. Sci. U.S.A. 84*, 3881−3885.
5. Rochet, J. C., and Lansbury, P. T., Jr. (2000) *Curr. Opin. Struct. Biol. 10*, 60−68.
6. Harper, J. D., and Lansbury, P. T., Jr. (1997) *Annu. Rev. Biochem. 66*, 385−407.
7. Dobson, C. M. (1999) *Trends Biochem. Sci. 24*, 329−332.
8. Iversen, L. L., Mortishire Smith, R. J., Pollack, S. J., and Shearman, M. S. (1995) *Biochem. J. 311*, 1−16.
9. Perutz, M. F., Finch, J. T., Berriman, J., and Lesk, A. (2002) *Proc. Natl. Acad. Sci. U.S.A. 99*, 5591−5595.
10. Sunde, M., and Blake, C. (1997) *Adv. Protein Chem. 50*, 123−159.
11. Astbury, W. T., Dickinson, S., and Bailey, K. (1935) *Biochem. J. 19*, 2354−2365.
12. Lansbury, P. T., Jr. (1999) *Proc. Natl. Acad. Sci. U.S.A. 96*, 3342−3344.
13. Bucciantini, M., Giannoni, E., Chiti, F., Baroni, F., Formigli, L., Zurdo, J., Taddei, N., Ramponi, G., Dobson, C. M., and Stefani, M. (2002) *Nature 416*, 507−511.
14. Pertinhez, T. A., Bouchard, M., Tomlinson, E. J., Wain, R., Ferguson, S. J., Dobson, C. M., and Smith, L. J. (2001) *FEBS Lett. 495*, 184−186.
15. Chiti, F., Webster, P., Taddei, N., Clark, A., Stefani, M., Ramponi, G., and Dobson, C. M. (1999) *Proc. Natl. Acad. Sci. U.S.A. 96*, 3590−3594.
16. Fandrich, M., Fletcher, M. A., and Dobson, C. M. (2001) *Nature 410*, 165−166.
17. Gross, M., Wilkins, D. K., Pitkeathly, M. C., Chung, E. W., Higham, C., Clark, A., and Dobson, C. M. (1999) *Protein Sci. 8*, 1350−1357.
18. Haass, C. (1998) *Molecular biology of Alzheimer's disease: genes and mechanisms involved in amyloid degeneration*, Harwood Academic Publishers, Amsterdam.
19. Gomez-Ramos, P., Mufson, E. J., and Moran, M. A. (1992) *Brain Res. 569*, 229−237.
20. Moran, M. A., Mufson, E. J., and Gomez-Ramos, P. (1993) *Acta Neuropathol. 85*, 362−369.
21. Mesulam, M. M., and Moran, M. A. (1987) *Ann. Neurol. 22*, 683−691.

22. Silver, A. (1974) *The Biology of Cholinesterases*, North-Holland, Amsterdam.
23. Massoulie, J., Pezzementi, L., Bon, S., Krejci, E., and Vallette, F. M. (1993) *Prog. Neurobiol. 41*, 31−91.
24. Soreq, H., and Seidman, S. (2001) *Nat. Rev. Neurosci. 2*, 294−302.
25. Small, D. H., Michaelson, S., and Sberna, G. (1996) *Neurochem. Int. 28*, 453−483.
26. Greenfield, S. A., and Vaux, D. J. T. (2002) *Neuroscience 113*, 485−492.
27. Kasa, P., Rakonczay, Z., and Gulya, K. (1997) *Prog. Neurobiol. 52*, 511−535.
28. Arendt, T., Bruckner, M. K., Lange, M., and Bigl, V. (1992) *Neurochem. Int. 21*, 381−396.
29. Geula, C., Mesulam, M. M., Saroff, D. M., and Wu, C. K. (1998) *J. Neuropathol. Exp. Neurol. 57*, 63−75.
30. Mesulam, M. M., and Geula, C. (1990) *Adv. Neurol. 51*, 235−240.
31. Smith, A. D., and Cuello, A. C. (1984) *Lancet 1*, 513.
32. Inestrosa, N. C., and Alarcon, R. (1998) *J. Physiol. 92*, 341−344.
33. Inestrosa, N. C., Alvarez, A., Perez, C. A., Moreno, R. D., Vicente, M., Linker, C., Casanueva, O. I., Soto, C., and Garrido, J. (1996) *Neuron 16*, 881−891.
34. Alvarez, A., Alarcon, R., Opazo, C., Campos, E. O., Munoz, F. J., Calderon, F. H., Dajas, F., Gentry, M. K., Doctor, B. P., De Mello, F. G., and Inestrosa, N. C. (1998) *J. Neurosci. 18*, 3213−3223.
35. Alvarez, A., Opazo, C., Alarcon, R., Garrido, J., and Inestrosa, N. C. (1997) *J. Mol. Biol. 272*, 348−361.
36. Munoz, F. J., and Inestrosa, N. C. (1999) *FEBS Lett. 450*, 205−209.
37. Schatz, C. R., Geula, C., and Mesulam, M. (1990) *Neurosci. Lett. 117*, 56−61.
38. Geula, C., and Mesulam, M. (1989) *Brain Res. 498*, 185−189.
39. Wright, C. I., Geula, C., and Mesulam, M. M. (1993) *Ann. N.Y. Acad. Sci. 695*, 65−68.
40. Shafferman, A., Kronman, C., Flashner, Y., Leitner, M., Grosfeld, H., Ordentlich, A., Gozes, Y., Cohen, S., Ariel, N., Barak, D., et al. (1992) *J. Biol. Chem. 267*, 17640−17648.
41. De Ferrari, G. V., Canales, M. A., Shin, I., Weiner, L. M., Silman, I., and Inestrosa, N. C. (2001) *Biochemistry 40*, 10447−10457.
42. Sonnhammer, E. L. L., and Durbin, R. (1995) *Gene 167*, GC1−GC10.
43. Wood, S. J., Maleeff, B., Hart, T., and Wetzel, R. (1996) *J. Mol. Biol. 256*, 870−877.
44. Huang, T. H., Yang, D. S., Plaskos, N. P., Go, S., Yip, C. M., Fraser, P. E., and Chakrabartty, A. (2000) *J. Mol. Biol. 297*, 73−87.
45. Fezoui, Y., Hartley, D. M., Harper, J. D., Khurana, R., Walsh, D. M., Condron, M. M., Selkoe, D. J., Lansbury, P. T., Jr., Fink, A. L., and Teplow, D. B. (2000) *Amyloid 7*, 166−178.
46. Klunk, W. E., Xu, C. J., and Pettegrew, J. W. (1994) *J. Neurochem. 62*, 349−354.
47. Jao, S. C., Ma, K., Talafous, J., Orlando, R., and Zagorski, M. G. (1997) *Amyloid 4*, 240−252.
48. Sudoh, S., Frosch, M. P., and Wolf, B. A. (2002) *Biochemistry 41*, 1091−1099.
49. LeVine, H., III (1999) *Methods Enzymol. 309*, 274−284.
50. Klunk, W. E., Jacob, R. F., and Mason, R. P. (1999) *Methods Enzymol. 309*, 285−305.
51. Mosmann, T. (1983) *J. Immunol. Methods 65*, 55−63.
52. Shearman, M. S., Ragan, C. I., and Iversen, L. L. (1994) *Proc. Natl. Acad. Sci. U.S.A. 91*, 1470−1474.
53. Fry, D. C., Fox, T. L., Lane, M. D., and Mildvan, A. S. (1985) *J. Am. Chem. Soc. 107*, 7659−7665.
54. Eaton, W. A., and Hofrichter, J. (1995) *Science 268*, 1142−1143.
55. El-Agnaf, O. M., Guthrie, D. J., Walsh, D. M., and Irvine, G. B. (1998) *Eur. J. Biochem. 256*, 560−569.
56. Pike, C. J., Overman, M. J., and Cotman, C. W. (1995) *J. Biol. Chem. 270*, 23895−23898.
57. Frenkel, D., Balass, M., and Solomon, B. (1998) *J. Neuroimmunol. 88*, 85−90.
58. Szendrei, G. I., Prammer, K. V., Vasko, M., Lee, V. M., and Otvos, L., Jr. (1996) *Int. J. Pept. Protein Res. 47*, 289−296.
59. Soto, C., Castano, E. M., Frangione, B., and Inestrosa, N. C. (1995) *J. Biol. Chem. 270*, 3063−3067.
60. Bon, S., Coussen, F., and Massoulie, J. (1997) *J. Biol. Chem. 272*, 3016−3021.
61. Bon, S., and Massoulie, J. (1997) *J. Biol. Chem. 272*, 3007−3015.
62. Perrier, A. L., Massoulie, J., and Krejci, E. (2002) *Neuron 33*, 275−285.
63. Giles, K. (1997) *Protein Eng. 10*, 677−685.
64. Altamirano, C. V., and Lockridge, O. (1999) *Biochemistry 38*, 13414−13422.
65. Altamirano, C. V., and Lockridge, O. (1999) *Chem.-Biol. Interact. 119−120*, 53−60.
66. Taylor, P., and Radic, Z. (1994) *Annu. Rev. Pharmacol. Toxicol. 34*, 281−320.
67. Reyes, A. E., Perez, D. R., Alvarez, A., Garrido, J., Gentry, M. K., Doctor, B. P., and Inestrosa, N. C. (1997) *Biochem. Biophys. Res. Commun. 232*, 652−655.
68. Fishman, E. B., Siek, G. C., MacCallum, R. D., Bird, E. D., Volicer, L., and Marquis, J. K. (1986) *Ann. Neurol. 19*, 246−252.
69. Siek, G. C., Katz, L. S., Fishman, E. B., Korosi, T. S., and Marquis, J. K. (1990) *Biol. Psychiatry 27*, 573−580.
70. Schegg, K. M., Harrington, L. S., Neilsen, S., Zweig, R. M., and Peacock, J. H. (1992) *Neurobiol. Aging 13*, 697−704.
71. Atack, J. R., Perry, E. K., Bonham, J. R., Perry, R. H., Tomlinson, B. E., Blessed, G., and Fairbairn, A. (1983) *Neurosci. Lett. 40*, 199−204.
72. Younkin, S. G., Goodridge, B., Katz, J., Lockett, G., Nafziger, D., Usiak, M. F., and Younkin, L. H. (1986) *Fed. Proc. 45*, 2982−2988.

BI0260334